atmosphere

MDPI

Article

Assimilating Satellite-Derived Snow Cover and Albedo Data to Improve 3-D Weather and Photochemical Models

Colleen Jones [1,*], Huy Tran [1,†], Trang Tran [1,‡] and Seth Lyman [1,2]

[1] Bingham Research Center, Utah State University, Vernal, UT 84078, USA; huy.tran@unc.edu (H.T.); ttran@ramboll.com (T.T.); seth.lyman@usu.edu (S.L.)
[2] Department of Chemistry and Biochemistry, Utah State University, Vernal, UT 84078, USA
* Correspondence: colleen.jones@usu.edu; Tel.: +1-435-722-1757
† Current address: Institute for the Environment, University of North Carolina, Chapel Hill, NC 27516, USA.
‡ Current address: Ramboll Environment and Health, Charlotte, NC 28273, USA.

Abstract: During wintertime temperature inversion episodes, ozone in the Uinta Basin sometimes exceeds the standard of 70 ppb set by the US Environmental Protection Agency. Since ozone formation depends on sunlight, and less sunlight is available during winter, wintertime ozone can only form if snow cover and albedo are high. Researchers have encountered difficulties replicating high albedo values in 3-D weather and photochemical transport model simulations for winter episodes. In this study, a process to assimilate MODIS satellite data into WRF and CAMx models was developed, streamlined, and tested to demonstrate the impacts of data assimilation on the models' performance. Improvements to the WRF simulation of surface albedo and snow cover were substantial. However, the impact of MODIS data assimilation on WRF performance for other meteorological quantities was minimal, and it had little impact on ozone concentrations in the CAMx photochemical transport model. The contrast between the data assimilation and reference cases was greater for a period with no new snow since albedo appears to decrease too rapidly in default WRF and CAMx configurations. Overall, the improvement from MODIS data assimilation had an observed enhancement in the spatial distribution and temporal evolution of surface characteristics on meteorological quantities and ozone production.

Keywords: MODIS; data assimilation; WRF; winter ozone; Uinta Basin

Citation: Jones, C.; Tran, H.; Tran, T.; Lyman, S. Assimilating Satellite-Derived Snow Cover and Albedo Data to Improve 3-D Weather and Photochemical Models. *Atmosphere* **2024**, *15*, 954. https://doi.org/10.3390/atmos15080954

Academic Editor: Aikaterini Bougiatioti

Received: 25 June 2024
Revised: 29 July 2024
Accepted: 7 August 2024
Published: 10 August 2024

1. Introduction

Ozone (O_3) in the troposphere negatively impacts respiratory health, especially for those with lung diseases [1]. The United States Clean Air Act of 1970 and the National Ambient Air Quality Standards establish the regulatory practices for planning and executing the reduction in O_3 precursor emissions to obtain the established air quality standard [2]. Tropospheric O_3 in Utah's Uinta Basin during wintertime temperature inversion episodes sometimes exceeds the standard of 70 ppb set by the US Environmental Protection Agency (EPA) [1,3], and the EPA declared portions of Uintah and Duchesne Counties below 6250 feet in elevation an O_3 nonattainment area in 2018 [4]. Only two places worldwide are known to experience wintertime O_3 exceeding EPA standards with any regularity. One is the Uinta Basin, and the other is Wyoming's Upper Green River Basin [5].

Atmospheric ozone formation occurs in the troposphere from reactions involving nitrogen (NO_x) oxides and volatile organic compounds (VOC). Most NO_x and VOC emissions are from oil and gas development in the Uinta Basin [6]. Wintertime temperature inversion conditions trap these pollutants near ground level. The increasing ground-level concentrations of pollutants and the photochemical reactions of these pollutants form tropospheric O_3 [7].

The number of ozone exceedance days in the Uinta Basin each year is closely tied to the local meteorology, especially snow cover and temperature inversions. Years with persistent

snow cover and high barometric pressure tend to have more days with strong winter inversions and high ozone concentrations. During inversion episodes, O_3 concentrations tend to be higher at lower elevations, where inversion conditions are stronger and last longer. In the absence of snow cover and winter inversions, O_3 concentrations in the Basin are similar to those in other rural, high-elevation locations around the western United States [7].

In areas in the US that do not comply with the federal O_3 standard, regulatory agencies are required to use 3-D photochemical transport models to test the efficacy of regulatory strategies to reduce the emissions of NO_x and VOC and the formation of O_3 [8,9]. While EPA has established guidelines for how to use models and other analyses to demonstrate attainment before strategy implementation [2], model outcomes are ultimately only as good as the models themselves.

Roth et al. [10] reviewed 18 model applications and found that two-thirds of the models applied for planning emission reduction strategies were inadequate due to limitations of air quality and meteorological databases and high uncertainties in the emission representation of the models [10]. Further, most modelers have found that the Weather Research and Forecasting (WRF) model's default configuration cannot capture the observed level of surface albedo (i.e., reflection of sunlight from the earth's surface). The maximum albedo simulated by WRF is less than 0.7, whereas an albedo above 0.8 are often observed in reality, including in the Uinta Basin when snow cover is present [11]. Underestimation of albedo will lead to inaccuracies in meteorological quantities and underestimation of photolysis rates and ozone formation. Because of this problem, most of the modeling studies for the Uinta Basin have implemented manual, snow-related corrections to the WRF model to increase the surface albedo outcome. Neemann, et al. [11] used a uniform albedo correction of 0.8 over the entire Basin; the resultant modeled albedo was unrealistically uniform. Most photochemical modelers after Neemann et al. have used this same approach [12,13].

Many researchers have successfully used Moderate-Resolution Imaging Spectroradiometer (MODIS) to improve WRF and photochemical model performance. For example, Werner et al. [14], compared pollution episodes in Eastern Europe and Poland during the summer and winter of 2017 during episodes of a poor forecast performance from the WRF-Chem model for $PM_{2.5}$ concentrations, and found that data assimilation of surface and MODIS satellite data improved model results and forecasting of $PM_{2.5}$. Ghude et al. [15] and Chen et al. [16], also demonstrated similar improvements in the forecast performance of $PM_{2.5}$ in Delhi, India, and the Atlantic Ocean, respectively. Parajuli et al. [17] found similar improvements in simulation with dust optical depth and aerosol optical depth when applying nudging with spectral MODIS satellite data to simulations in the Middle East and North Africa. The validation results of Endale et al. [18] indicated that the aerosol optical depth of MODIS-terra over Dire Dawa, Ethiopia, showed the best correlation with multispectral satellite sensors with differences in performance by season. All seasons had higher aerosol optical depth except during winter [18].

Zhang et al. [19] showed that ensemble assimilation of precipitation-affected radiance improved the quality of precipitation forecasts, including intensity and spatial distribution, when verified by independent, ground-based precipitation observations. Paul et al. [20] demonstrated improved performance for regional monsoonal rainfall by incorporating spectral nudging to reduce bias in the simulation of deforested regions in Central India. Meng et al. [21] improved the systematic cold bias of WRF temperature modeling for the Tibetan Plateau by assimilating albedo data from WRF. Kim and Kim [22] assimilated satellite radiance data to improve WRF performance in the Arctic. Ran et al. [23–25] used MODIS data assimilation to improve the simulation of meteorology and air quality.

The primary motivation for this study was to improve weather models of winter temperature inversion and photochemical models of O_3 formation by assimilating remote sensing observations. This study achieves this by incorporating MODIS's surface albedo and snow cover data into the WRF and CAMx models. The novelty of this study is that it applies MODIS remote sensing data to models of periods with winter O_3 formation

and investigates the impacts of data assimilation on the models' performance. Improved models increase the potential value of regulatory strategies to attain ambient air quality standards that depend on model performance.

2. Materials and Methods

2.1. Study Area

The Uinta Basin (Figure 1) in northeastern Utah, USA is one of a few places experiencing high O_3 concentrations closely tied to the local meteorology of snow cover and temperature inversions [5–7]. The years with persistent snow cover and high barometric pressure tend to have more days with strong winter inversions and high ozone concentrations. During inversion episodes, O_3 concentrations tend to be higher at lower elevations, where inversion conditions are stronger and last longer. In the absence of snow cover and winter inversions, O_3 concentrations in the Basin are similar to those in other rural, high-elevation locations around the western United States [7].

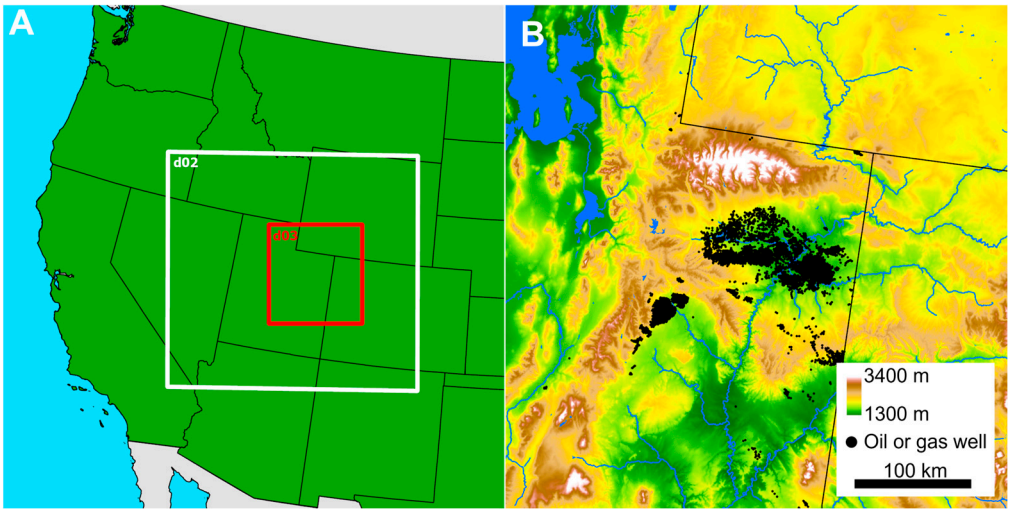

Figure 1. WRF one-way nested 12-4-1.33 km domains (**A**) and details of a 1.33 km domain, including topography and location of oil and gas wells (**B**). The white rectangle is Domain 2 and the red rectangle is Domain 3 from Table 4.

2.2. Data Sources

The Moderate-Resolution Imaging Spectroradiometer (MODIS) is a National Aeronautics and Space Administration (NASA) (White Sands, New Mexico, USA) satellite-based instrument with high radiometric sensitivity in 36 spectral bands ranging from 0.4 µm to 14.4 µm, and MODIS data used in this study were accessed from NASA's MODIS website [26]. Table 1 describes the MODIS datasets utilized for this study.

Table 1. List and description of MODIS datasets applied in this study.

Dataset	Reference	Descriptions	Horizontal Resolution	Temporal Resolution
MCD43A1	Schaaf [27]	MODIS Terra + Aqua BRDF/Albedo Model Parameters Daily L3 Global—500 m V006	500 m	Daily
MCD19A1	Lyapustin [28]	MODIS Terra + Aqua Land Surface BRF Daily L2G Global 500 m, 1 km and 10 km S.I.N. Grid V006	500 m	Daily

Table 1. *Cont.*

Dataset	Reference	Descriptions	Horizontal Resolution	Temporal Resolution
MCD19A2	Lyapustin [29]	MODIS Terra + Aqua Land Aerosol Optical Thickness Daily L2G Global 1 km S.I.N. Grid V006	1 km	Daily
MOD10A1/MYD10A1	Hall [30]	MODIS Terra + Aqua Snow Cover Daily L3 Global 500 m Grid. Only MOD10A1 is used	500 m	Daily
MCD15A3H	Myneni [31]	MODIS Terra + Aqua Leaf Area Index/FPAR 4-Day L4 Global 500 m (4 days composite)	500 m	Daily

Meteorological and ozone data used for comparison were from Lyman and Tran [7] and were collected as described therein.

2.3. Data Analysis Methods

Figure 2 explains the method used to assimilate MODIS data into the WRF and CAMx models. All MODIS data from their original horizontal resolution (500 m or 1 km) were re-gridded to the model resolution of 1.3 km using the Earth System Modeling Framework. The Second Simulation of a Satellite Signal in the Solar Spectrum vector code (6SV) was utilized to construct a lookup table for the diffuse radiation fraction, which was then used in the bidirectional reflectance distribution function (BRDF) albedo to determine diurnal values of snow and spectrum shortwave albedo.

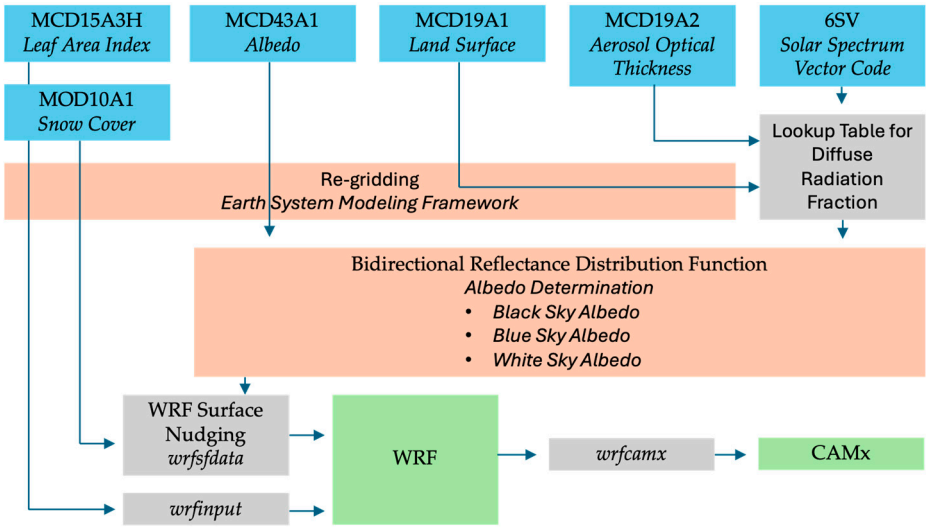

Figure 2. Diagram of the MODIS data assimilation into the WRF and CAMx models.

Except for the MODIS Leaf Area Index (LAI), which replaces the original and climatology seasonal LAI variable in WRF's input file, this study incorporated all other MODIS-derived quantities in the WRF surface nudging module before entering the WRF core model. Finally, this study used the wrfcamx module to process WRF outputs and prepare meteorology inputs in binary format for CAMx.

This study adapted specific WRF and CAMx model source codes to incorporate MODIS data assimilation (see Tables S1 and S2 for specifics). One notable aspect of this approach is the integration of MODIS data using the WRF surface nudging module (wrfsfdda). This allowed this study to leverage various standard options for controlling data assimilation. These options include toggling data assimilation on or off, adjusting

the frequency of replacing WRF estimates with MODIS data, modifying weighting factors, ramping times, and more.

2.4. Re-Gridding MODIS Data to the WRF Model Domain

This study applied the Earth System Modeling Framework (ESMF5F) to the NCAR Command Language (NCL6F) front end to re-grid MODIS data from their original horizontal resolution (Table 1) to the WRF horizontal resolution of 1.3 km. Several interpolation methods are supported by ESMF, including "*bilinear*", "*patch*", "*conserve*", and "*neareststod/nearestdtos*". Sensitivity tests suggested the "*conserve*" method produces the best preservation of MODIS data in the WRF domain. Since the resolution of the MODIS grid is higher than that of the WRF, the downscaling of MODIS data to the WRF grid involves minimum interpolation, which explains the better performance of the "*conserve*" method over other interpolation methods.

2.5. Determining Diurnal Surface Albedo from the MODIS MCD43A1 Dataset

MODIS MCD43A1 provides weighting parameters associated with the *RossThick-LiSparseReciprocal* bidirectional reflectance distribution function (BRDF) that best describes the anisotropy of each pixel. These parameters are used to estimate black sky (α_{BSA}) and white sky (α_{WSA}) albedo for any solar zenith angle (θ_{Sun}), model weighting parameters (*iso* = *isotropic*, *vol* = *volumetic*, and *geo* = *geometic*) and selected bin of wavelength (λ) using the following equations:

$$\alpha_{BSA}(\theta_{Sun},\ \lambda) \ = \ f_{iso}(\lambda)g_{iso}(\theta_{Sun}) + f_{vol}(\lambda)g_{vol}(\theta_{Sun}) + f_{geo}(\lambda)g_{geo}(\theta_{Sun}) \quad (1)$$

$$\alpha_{WSA}(\lambda) \ = \ f_{iso}(\lambda)g_{3iso} + f_{vol}(\lambda)g_{3vol} + f_{geo}(\lambda)g_{3geo} \quad (2)$$

Blue sky albedo (α_{BLUE}) refers to albedo calculated under real-world conditions with a combination of diffuse and direct lighting based on atmospheric and view-geometry conditions. Blue sky albedo can be determined by:

$$\alpha_{BLUE} \ = \ \alpha_{BSA}(1 - D) + \alpha_{WSA}D \quad (3)$$

Parameters on the right-hand side of Equations (1) and (2) are provided by MCD43A1. The Second Simulation of a Satellite Signal in the Solar Spectrum–Vector (6SV8F) model calculates the split factor *D* between diffuse and direct lighting [32]. Although 6SV simulates diffuse and direct effects under different atmospheric and surface conditions, the specified parameters in the model, as shown in Table 2, with the assumption that these parameters best represent winter conditions in the Uintah Basin.

Table 2. Parameter settings used as inputs for 6SV model to calculate the split factor D between diffuse and direct lighting [32].

Parameters	Values	Descriptions
Atmospheric profile	3	Midlatitude winter
Aerosol model	1	Continental model
Sensor level	1000 km	Set to satellite altitude
Ground reflectance type	0	Homogenous surface
Directional effect	1	Directional effect is considered
Directional effect model	10	MODIS operational BDRF
Weigh factors for MODIS BDRF	1.0, 0.77, 0.2	Weights for Lambertian kernel, RossThick kernel, LiSparse kernel in MODIS BDRF
Atmospheric correction mode	−1	No atmospheric correction

Other inputs of the 6SV model, including view angles (zenith θ_{View}, and azimuth ϑ_{View}) are taken from MCD19A1, and aerosol optical depth (AOD) is taken from MCD19A2. Al-

though MCD19A2 is a daily dataset, its coverage is sporadic (i.e., not all pixels covering the model domain are available in each scan). Therefore, a monthly average AOD was derived from MCD19A2 to produce complete coverage over the WRF model domain. This study used the 6SV model to create a lookup table for D values for a wide range of wavelengths, solar angles, view angles, and aerosol optical depth (λ, θ_{solar}, ϑ_{solar}, θ_{view}, AOD).

2.6. WRF Model Configurations

For the reference simulation (referred to as REF), this study used the well-tested grid definitions, topography, land use, boundary/initial conditions, and physics options described in Tables 3–5, and Figure 1. These configurations are the same as the 2017 Air Resource Management Strategy (ARMS) modeling study [33], except that surface data nudging was not used in the current study. The modeling episode was from 1 to 28 February 2011, divided into four 5.5-day batches and one 8.5-day batch. The first 12 h of each batch served as spin-up time and were discarded from the analysis. This period covered three distinct inversion events around 4–9 February, 12–17 February and 21–25 February.

Table 3. Grid definitions for the WRF Preprocessor System.

Parameter Name	Parameter Value
Projection	Lambert conformal
Reference latitude	40 N
Reference longitude	−97 W
truelat1	33
truelat2 =	45
stand_lon =	−97
ref_x	190.5
ref_y	90.5

Table 4. WRF model grid configurations and topographical, land use, and initial/boundary conditions.

	Domain 1	Domain 2	Domain 3
Grid size (x, y)	201 × 191	253 × 253	298 × 322
Vertical levels	37	37	37
Vertical coordinates	Terrain-following Eta (non-hybrid)	Terrain-following Eta (non-hybrid)	Terrain-following Eta (non-hybrid)
Vertical grid spacing	12–16 m in boundary layer	12–16 m in boundary layer	12–16 m in boundary layer
Horizontal resolution (km)	12	4	1.33
Model time step (s)	25	8.33	2.77
Topographic dataset	USGS GTOPO30	USGS GTOPO30	USGS GTOPO30
Land use dataset	NLCD2011 modified 9s	NLCD2011 modified 9s	NLCD2011 modified 9s
Initial and boundary conditions	N.A.M.-12 km	Continuous updates nested from 12 km domain	Continuous updates nested from 4 km domain
Top and bottom boundary conditions	- Top: Rayleigh dampening for the vertical velocity - Bottom: physical, non free-slip option	- Top: Rayleigh dampening for the vertical velocity - Bottom: physical, non free-slip option	- Top: Rayleigh dampening for the vertical velocity - Bottom: physical, non free-slip option
Veg parm table variables modified for winter simulations	SNUP, MAXALB	SNUP, MAXALB	SNUP, MAXALB
Snow cover initialization	- SNODAS	- SNODAS	- SNODAS

Table 5. Physics options used in the WRF.

WRF Treatment	Option Selected
Microphysics	Thompson
Longwave Radiation	RRTMG
Shortwave Radiation	RRTMG
Land Surface Model (LSM)	NOAH
Planetary Boundary Layer (PBL) Scheme	MYJ
Cumulus Parameterization	Kain–Fritsch in the 12 km domains. None in the 4 and 1.3 km domain.

2.7. CAMx Model Configurations

This study used the Comprehensive Air Quality Model (CAMx) version 6.59F in the same configuration as the 2017 Air Resource Management Strategy (ARMS) modeling study [33] in its finest domain (1.3 km), which is presented as *d03* in Figure 1. Table 6 provides details on the CAMx domain configurations. The Utah Department of Environmental Quality's emission inventory for oil and gas production in the Uintah Basin in 2014 (UBEI2014) was processed using Sparse Matrix Operator Kerner Emissions (SMOKE) version 4.510F (Community Modeling and Analysis System, Chapel Hill, NC, USA) and projected to model episode 1 to 28 February 2011, with scaling factors derived from oil and gas production rates in 2014 and 2011, to provide emissions for the CAMx run.

Table 6. Summary of CAMx model configurations.

Science Options	Configuration
Model Code Version	CAMx V6.5
Horizontal Grid	1.33 km (298 × 322)
Vertical Grid	25 vertical layers
Initial and Boundary Conditions	Processed from ARMS2017
Boundary Conditions	12 km BCs from WAQS 2011b
Land-Use Data	Land-use fields from meteorological model
Photolysis Rate Preprocessor	TUV V4.8 (Clear sky photolysis rates from TOMS data)
Gas-Phase Chemistry	CB6r4
Aerosol Phase	CF (coarse- and fine-mode aerosols)
Diffusion Scheme	
Horizontal Grid	Explicit horizontal diffusion
Vertical Grid	K-theory 1st-order closure
Deposition Scheme	
Dry Deposition	ZHANG03 with modifications based on [34]
Wet Deposition	CAMx-specific formulation
Numerical Solvers	
Gas-phase Chemistry	Euler Backward Iterative (E.B.I.) solver
Horizontal Advection	Piecewise Parabolic Method (P.P.M.)
Vertical Advection	Implicit scheme with vertical velocity update

2.8. Implementation of MODIS Data Assimilation to the WRF/CAMx Model Platform

2.8.1. WRF Model Modification

This study modified specific WRF source codes to allow the model to assimilate MODIS surface albedo and snow cover. Notably, this study implemented the assimilation to WRF through WRF's surface assimilation module, which enables the WRF modeler to turn MODIS data assimilation on or off and to control assimilation frequency (e.g., every 1, 2, 6 h, or longer). As a component of the surface assimilation model, the surface albedo was also controlled by other standard options in the WRF *fdda* module. New variables (see Supplementary Materials Tables S1 and S2) were added to the input file of the *wrfsfdda* module (*wrfsfdda_d<domain>).* Unlike hourly surface albedo, which has a diurnal cycle after being processed as described in Section 2.2, the hourly snow cover is aggregated from

the MODIS re-gridded daily snow cover data, which means all hours within the same date have identical snow cover values.

MODIS snow cover and LAI were also written to the WRF input files (*wrfinput_d<domain>*). MODIS LAI replaced the default climatology LAI in *wrfinput*, which often is incorrect and in coarse resolution. In WRF simulation, LAI was read in from *wrfinput* as an initial condition and evolved with other simulated parameters such as snow depth and snow cover.

2.8.2. CAMx Model Modification

Although CAMx reads in most of the meteorological inputs from WRF output files, CAMx determines its own albedo and snow cover as the functions of snow water equivalent, snow age, and land-use type. This means WRF albedo and snow cover improvements are not carried over to CAMx in the standard model configuration. To force CAMx to use MODIS-assimilated data from WRF, CAMx code modifications were made (see Supplementary Materials Tables S1 and S2). These included modifications to the *wrfcamx* module so that the MODIS albedo and snow cover are written to CAMx inputs.

If no information about snow age is available, CAMx assumes an albedo of near-fresh snow conditions. Therefore, CAMx-albedo may be higher than that estimated by WRF before decreasing gradually as the snow ages. This implies that the albedo calculated by the CAMx model in standard configuration could be higher than the albedo value taken from WRF inputs.

3. Results

3.1. Impact of MODIS Data Assimilation on WRF Model Performance

Figure 3 compares surface albedo simulated in the WRF default configuration (referred to as REF hereafter) to WRF simulations that included MODIS data assimilation (referred to as MODIS hereafter) as an average across 1–28 February 2011. Compared to REF, MODIS not only gives higher albedo in the Uinta Basin, but the spatial distribution of albedo is more realistic. A comparison of the snow cover fraction in Figure 4 shows that, while snow cover in the Uinta Basin is somewhat lower in MODIS than in REF, its distribution is more realistic. In REF, snow cover is more complete and more uniform at many locations in the model. Initialization of the model with the SNODAS data product [35] could be one of the reasons for the snow cover distribution in REF.

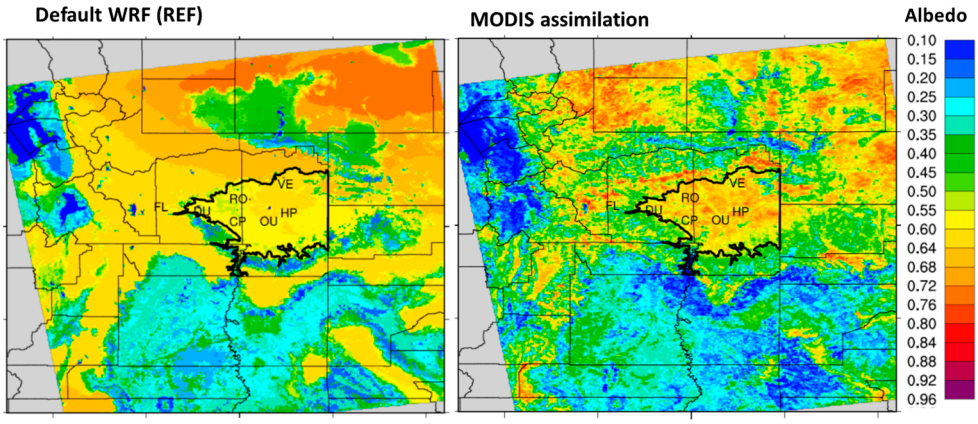

Figure 3. Comparison of the surface albedo fraction obtained in simulations using the WRF default configuration (**left**) and MODIS data assimilation (**right**). (Thin black lines = county outlines; heavy black outline = Uinta Basin ozone nonattainment area; and two-letter abbreviations = air quality monitoring stations.)

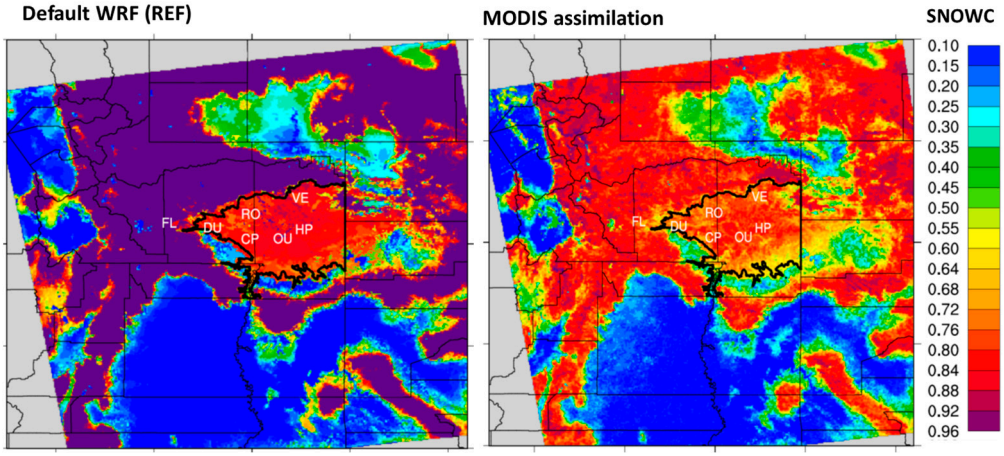

Figure 4. Comparison of snow cover fraction (SNOWC) obtained in simulations using the WRF default configuration (**left**) and MODIS data assimilation (**right**). (Thin black lines = county outlines; heavy black outline = Uinta Basin ozone nonattainment area; and two-letter abbreviations = air quality monitoring stations.)

Figure 5 compares the time evolution of WRF estimates of snow depth, snow water equivalent, and snow cover between the REF and MODIS cases as an average over six locations in the Uinta Basin. This figure shows that every time WRF was re-initialized with SNODAS data (indicated by green bars), snow depth, snow water equivalent, and snow cover sharply increased. This result was observed in REF and MODIS, as they were both periodically re-initialized with SNODAS data. All three parameters tended to decay faster in REF than in MODIS. Also, from 11 February onward, several storms brought extra snow to the Basin, and WRF consistently estimated more snow in REF than in MODIS. The zigzag-like snow cover pattern in MODIS in Figure 5 is the effect of data assimilation, as the snow cover fraction was directly taken from the MODIS dataset. Snow cover was typically higher in REF than in MODIS, likely caused by SNOWDAS data reinitialization. The conclusion is that snow-related characteristics were retained longer in MODIS than in REF for extended simulations and without reinitialization.

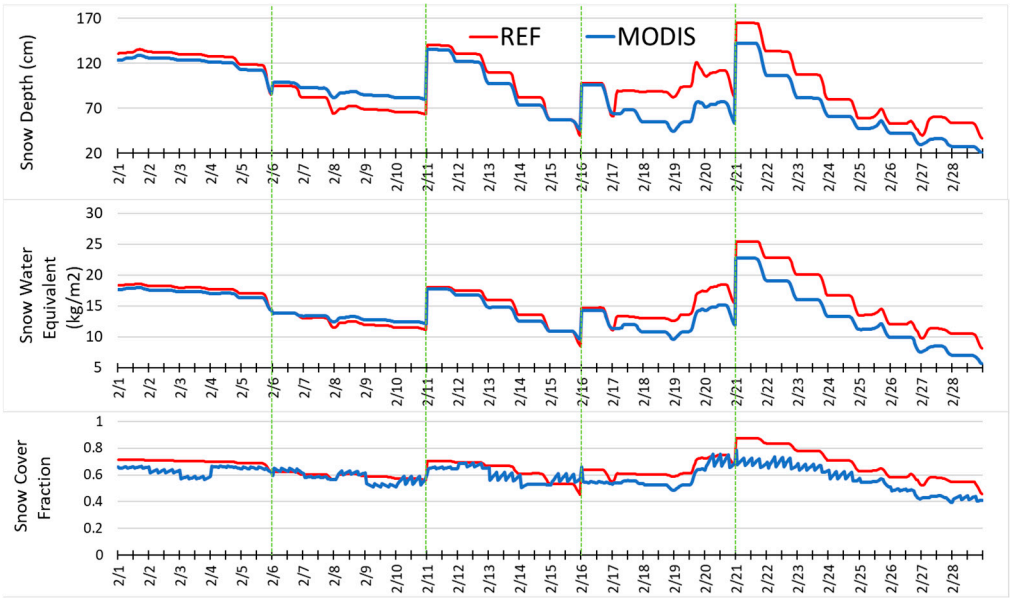

Figure 5. Comparison of snow cover fraction, snow water equivalent, and snow depth using the WRF default configuration (REF) and MODIS data assimilation (MODIS). Green bars show periods where WRF reinitialized snow characteristics using the SNOWDAS dataset.

Planetary boundary layer height is the height of the mixed layer of the atmosphere that is in direct contact with the earth's surface. The lapse rate is a measure of inversion strength. This study found no meaningful differences in the planetary boundary layer height and lapse rate between REF and MODIS at Ouray (Figure 6). Boundary layer height tended to be slightly shallower in MODIS compared to REF, but the lapse rate was slightly weaker in MODIS. Figure S1 shows a comparative time series for other meteorological parameters, as well as statistical analyses including mean absolute error (MAE), bias (BIAS), and index of agreement (IOA). Overall, the MODIS data assimilation technique did not consistently result in better WRF performance. One exception was the simulation of wind speed (Figure S1). On some days when storm fronts passed through the Basin, the REF simulation estimated unrealistically high wind speed, whereas wind speeds were lower and closer to observed values in the MODIS simulation.

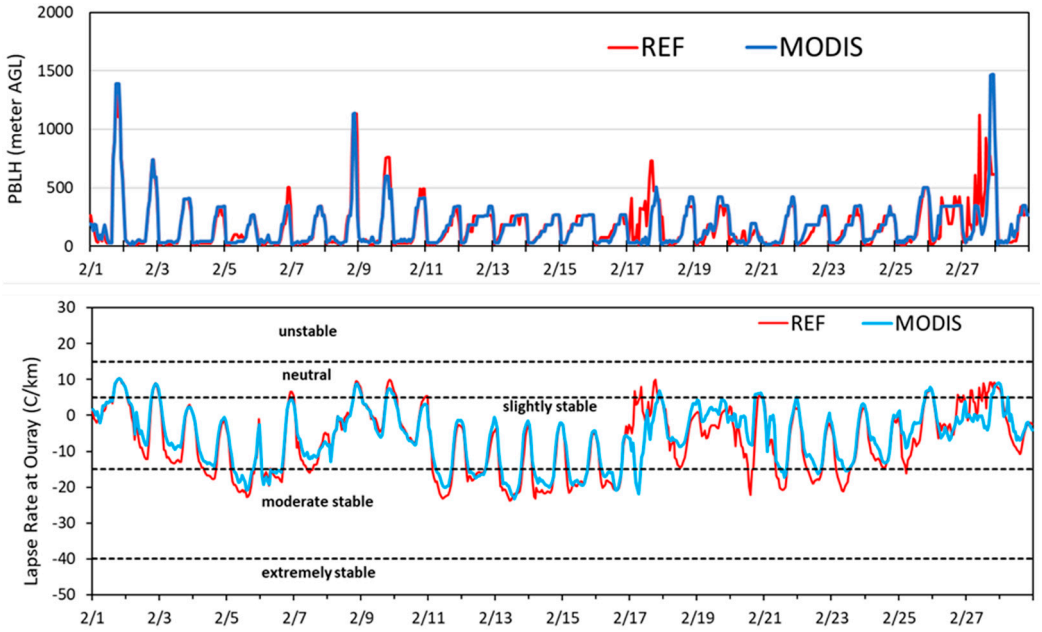

Figure 6. Comparison of planetary boundary layer height (P.B.L.H.) and lapse rate using the WRF default configuration (REF) and MODIS data assimilation (MODIS).

3.2. Impact of MODIS Data Assimilation on CAMx Model Performance

Figure 7 compares the photolysis rate of ozone at Ouray in REF and MODIS. From 1–10 February, no new snow was simulated in the model. Since snow tends to decay quicker in the REF simulations than in the MODIS simulations, the photolysis rate in the MODIS simulations exceeded that in REF at the end of this period. However, on 11 February and afterward (indicated as the part of the figure to the right of the green vertical bar), as new snow was estimated in WRF, and because of the fresh-snow effect in CAMx, the photolysis rate in REF was consistently higher than in MODIS. This shows that the higher albedo obtained in WRF with the MODIS satellite data assimilation technique did not necessarily translate to a higher photolysis rate in the CAMx model. A positive effect of MODIS data assimilation on the CAMx photolysis rate could be expected if the simulation included an extended period where no new snow was simulated. Additionally, an online coupling meteorology-and-chemistry model such as WRF-Chem may benefit more from MODIS data assimilation than a decoupled model platform such as WRF-CAMx.

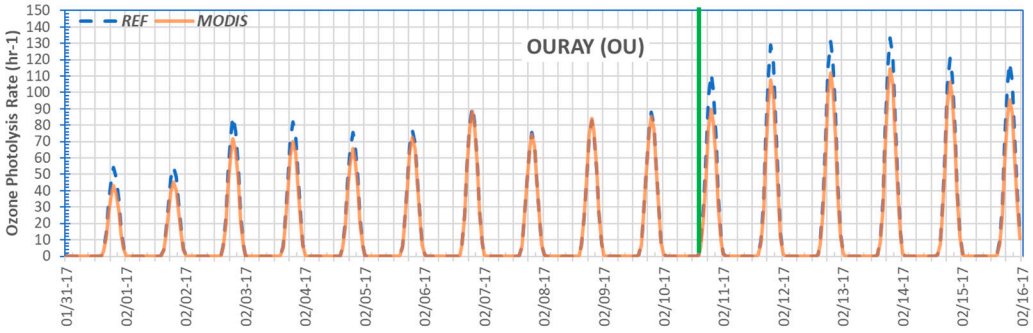

Figure 7. Comparison of photolysis rates simulated by CAMx using the default configuration (REF) and MODIS data assimilation (MODIS). (Green line = a new snow event.)

As expected from the photolysis rate comparison, this study found similar patterns in ozone concentrations between the REF and MODIS simulations. Simulated ozone, as shown in Figure 8 for the Ouray air quality monitoring station, was related to the photolysis rate shown in Figure 7. Neither scenario simulated ozone at levels observed during this episode, probably because of challenges with model emissions and chemistry, which also impact winter O_3 [13].

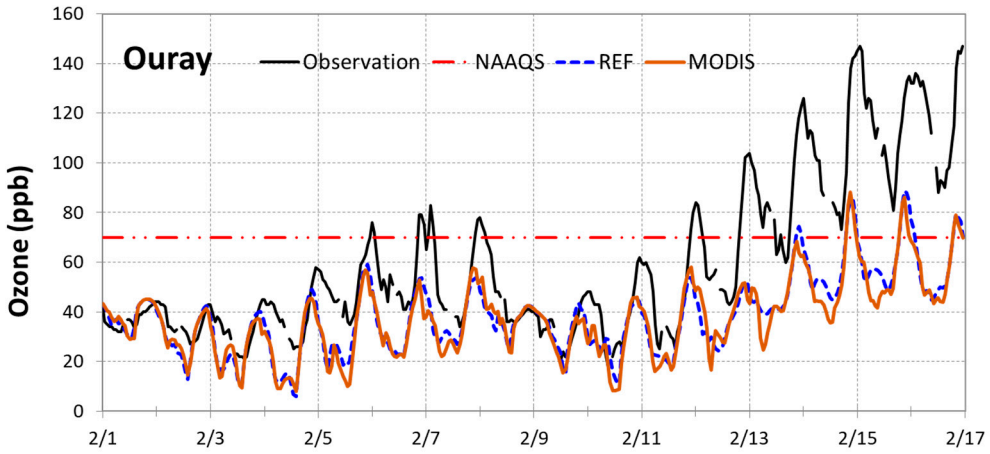

Figure 8. Comparison of ozone at Ouray as simulated by CAMx using the default configuration (REF) and MODIS data assimilation (MODIS). (Red dash line = EPA National Ambient Air Quality Standard (NAAQS) for ozone).

4. Discussion

Meng et al. [21] utilized MODIS to improve the accuracy of albedo simulation and their impact on regional climate models and global atmospheric general circulation models in the Tibetan Plateau. They demonstrated that the overestimation of snow cover causes an overestimation of surface albedo and cold temperature bias. The age of the snow also contributes to the overestimation of surface albedo, and light-absorbing aerosols could also be influencing model results [21]. Both Meng et al. [21] and our study involve assimilating MODIS albedo data into models to assess the impact of model outputs or simulations on understanding precipitation or ozone formation dynamics, respectively.

Ran et al. [24] also used MODIS albedo data assimilation as well as vegetation data assimilation to improve the representation of soil nitric oxide (NO) emissions in the Community Multiscale Air Quality (CMAQ) and their implications for air quality. They found that surface O_3 was biased high for April, August, and October and that MODIS vegetation data did improve their simulations during the growing season. WRF/CMAQ models used in their study had improvements in temperature, humidity, wind, and O_3 simulations [24]. While all studies contribute to advancing modeling capabilities by integrating high-resolution remote sensing data, the Uinta Basin study provides critical insights into

real-world O_3 exceedances and regulatory challenges during wintertime inversions and snow cover.

Improvements to WRF simulation of surface albedo and snow cover were substantial. However, the impact of MODIS data assimilation on WRF performance for other meteorological quantities was minimal. The contrast between the data assimilation and reference cases may have been greater for a period with no new snow since albedo appears to decrease too rapidly in default WRF and CAMx configurations. Overall, the improvement from MODIS data assimilation was too small to impact meteorological quantities and ozone production significantly. Tran et al. [13] found that the assimilation of surface and vertical meteorological data led to improvements in WRF performance, and a combination of the approach of Tran et al. with the MODIS data assimilation performed in this work could maximize the quality and representativeness of the model at the Basin-wide scale.

Additional satellite-based datasets could be used to improve WRF and CAMx performance further. For example, using the same framework developed in this project, model cloud cover could be improved, or solar attenuation by aerosols could be more accurately accounted for.

5. Conclusions

This study addresses the complex formation of wintertime O_3 in Utah's Uinta Basin, focusing on the impact of MODIS remote sensing data assimilation on the performance of atmospheric models. Our findings reveal significant insights into the interplay between model configurations, meteorological phenomena, and the role of MODIS data in improving model performance. By integrating MODIS-derived surface albedo and snow cover data into the WRF and CAMx model frameworks, we observed notable enhancements in the spatial distribution and temporal evolution of surface characteristics. MODIS assimilation led to more realistic representations of snow cover, albedo, and photolysis rates, thereby improving the accuracy of O_3 simulations.

Despite the improvements achieved through MODIS data assimilation, several limitations persist in our modeling approach. Uncertainties in emission inventories, model physics, and chemical mechanisms warrant further investigation to enhance model fidelity. Additionally, future studies should explore the potential of online coupled meteorology-chemistry models, such as WRF-Chem, to capitalize on the benefits of MODIS data assimilation for comprehensive air quality assessments.

The findings of this study have significant implications for air quality management and regulatory practices in the Uinta Basin. Accurate modeling of O_3 formation processes is essential for developing effective mitigation strategies and attainment plans to meet National Ambient Air Quality Standards. By incorporating MODIS data assimilation techniques into atmospheric models, regulatory agencies can enhance their understanding of O_3 dynamics and optimize emission reduction measures to achieve air quality goals.

Supplementary Materials: The following supporting information can be downloaded at: https://www.mdpi.com/article/10.3390/atmos15080954/s1, Table S1: Summary of WRF model modifications.; Table S2: Summary of CAMx model modifications.; Figure S1: Comparison of the overall performance of WRF using the WRF default configuration (REF) and MODIS data assimilation (MODIS). Observed values are also shown. The panels show water vapor mixing ratio, temperature at 2 m above ground, wind speed at 10 m, and wind direction at 10 m (in descending order). Skill scores are shown at the bottom of each boxplot (REF/MODIS; see text for an explanation of scores). The green boxes indicate the days when storm fronts passed through the Basin.

Author Contributions: Conceptualization, H.T.; methodology, H.T.; validation, H.T. and T.T.; formal analysis, H.T.; data curation, H.T., T.T. and C.J.; writing—original draft preparation, H.T., T.T. and C.J.; writing—review and editing, C.J. and S.L.; funding acquisition, H.T. and S.L. All authors have read and agreed to the published version of the manuscript.

Funding: This study was funded by the Utah Division of Air Quality, Uintah Special Service District 1, and the Utah Legislature.

Institutional Review Board Statement: Not applicable.

Informed Consent Statement: Not applicable.

Data Availability Statement: The data presented in this study are available in NASA EarthData at https://ladsweb.modaps.eosdis.nasa.gov/ (11 September 2020) [27–31]. These data were derived from the following resources available in the public domain: https://ladsweb.modaps.eosdis.nasa.gov/missions-and-measurements/products/MCD43A1, 11 September 2020; https://ladsweb.modaps.eosdis.nasa.gov/missions-and-measurements/products/MCD19A1, accessed on 11 September 2020; https://ladsweb.modaps.eosdis.nasa.gov/missions-and-measurements/products/MCD19A2, accessed on 11 September 2020; https://modis-snow-ice.gsfc.nasa.gov/?c=MOD10A1; accessed on 11 September 2020; https://ladsweb.modaps.eosdis.nasa.gov/missions-and-measurements/products/MCD15A3H, accessed on 11 September 2020.

Conflicts of Interest: The authors declare no conflict of interest.

References

1. USEPA. Ground-Level Ozone Pollution. Available online: https://www.epa.gov/ground-level-ozone-pollution (accessed on 20 September 2023).
2. USEPA. *Guidance on the Use of Models and Other Analyses in Attainment Demonstrations for the 8-Hour Ozone NAAQS*; EPA-454/R-05-002; USEPA: Washington, DC, USA, 2005.
3. USEPA. *National Ambient Air Quality Standards for Ozone Final Rule*; Environmental Protection Agency: Washington, DC, USA, 2015; pp. 1–178.
4. McCarthy, J.E.; Shouse, K.C. Implementing EPA's 2015 ozone air quality standards. *CRS Rep.* **2018**, *43092*.
5. Oltmans, S.; Schnell, R.; Johnson, B.; Pétron, G.; Mefford, T.; Neely, R., III. Anatomy of wintertime ozone associated with oil and natural gas extraction activity in Wyoming and Utah. *Elementa* **2014**, *2*, 000024. [CrossRef]
6. Edwards, P.M.; Brown, S.S.; Roberts, J.M.; Ahmadov, R.; Banta, R.M.; DeGouw, J.A.; Dubé, W.P.; Field, R.A.; Flynn, J.H.; Gilman, J.B. High winter ozone pollution from carbonyl photolysis in an oil and gas basin. *Nature* **2014**, *514*, 351–354. [CrossRef]
7. Lyman, S.; Tran, T. Inversion structure and winter ozone distribution in the Uintah Basin, Utah, USA. *Atmos. Environ.* **2015**, *123*, 156–165. [CrossRef]
8. USEPA. Controlling Air Pollution from the Oil and Naturual Gas Industry. Available online: https://www.epa.gov/controlling-air-pollution-oil-and-natural-gas-industry (accessed on 6 August 2024).
9. USEPA. Controlling Air Pollution from Oil and Natural Gas Operations. Available online: https://www.epa.gov/controlling-air-pollution-oil-and-natural-gas-operations (accessed on 19 May 2024).
10. Roth, P.M.; Reynolds, S.D.; Tesche, T.W. Air Quality Modeling and Decisions for Ozone Reduction Strategies. *J. Air Waste Manag. Assoc.* **2005**, *55*, 1558–1573. [CrossRef]
11. Neemann, E.M.; Crosman, E.T.; Horel, J.D.; Avey, L. Simulations of a cold-air pool associated with elevated wintertime ozone in the Uintah Basin, Utah. *Atmos. Chem. Phys.* **2015**, *15*, 135–151. [CrossRef]
12. Matichuk, R.; Tonnesen, G.; Luecken, D.; Gilliam, R.; Napelenok, S.L.; Baker, K.R.; Schwede, D.; Murphy, B.; Helmig, D.; Lyman, S.N. Evaluation of the Community Multiscale Air Quality Model for Simulating Winter Ozone Formation in the Uinta Basin. *J. Geophys. Res. Atmos.* **2017**, *122*, 13545–13572. [CrossRef]
13. Tran, T.; Tran, H.; Mansfield, M.; Lyman, S.; Crosman, E. Four dimensional data assimilation (FDDA) impacts on WRF performance in simulating inversion layer structure and distributions of CMAQ-simulated winter ozone concentrations in Uintah Basin. *Atmos. Environ.* **2018**, *177*, 75–92. [CrossRef]
14. Werner, M.; Kryza, M.; Guzikowski, J. Can Data Assimilation of Surface PM2.5 and Satellite AOD Improve WRF-Chem Forecasting? A Case Study for Two Scenarios of Particulate Air Pollution Episodes in Poland. *Remote Sens.* **2019**, *11*, 2364. [CrossRef]
15. Ghude, S.D.; Kumar, R.; Jena, C.; Debnath, S.; Kulkarni, R.G.; Alessandrini, S.; Biswas, M.; Kulkrani, S.; Pithani, P.; Kelkar, S. Evaluation of PM2. 5 forecast using chemical data assimilation in the WRF-Chem model: A novel initiative under the Ministry of Earth Sciences Air Quality Early Warning System for Delhi, India. *Curr. Sci* **2020**, *118*, 1803–1815. [CrossRef]
16. Chen, D.; Liu, Z.; Davis, C.; Gu, Y. Dust radiative effects on atmospheric thermodynamics and tropical cyclogenesis over the Atlantic Ocean using WRF-Chem coupled with an AOD data assimilation system. *Atmos. Chem. Phys.* **2017**, *17*, 7917–7939. [CrossRef]
17. Parajuli, S.P.; Yang, Z.-L.; Lawrence, D.M. Diagnostic evaluation of the Community Earth System Model in simulating mineral dust emission with insight into large-scale dust storm mobilization in the Middle East and North Africa (MENA). *Aeolian Res.* **2016**, *21*, 21–35. [CrossRef]
18. Endale, T.A.; Raba, G.A.; Beketie, K.T.; Feyisa, G.L. Exploring the Trend of Aerosol Optical Depth and its Implication on Urban Air Quality Using Multi-spectral Satellite Data During the Period from 2009 to 2020 over Dire Dawa, Ethiopia. *Nat. Environ. Pollut. Technol.* **2024**, *23*, 1–15. [CrossRef]

19. Zhang, S.Q.; Zupanski, M.; Hou, A.Y.; Lin, X.; Cheung, S.H. Assimilation of Precipitation-Affected Radiances in a Cloud-Resolving WRF Ensemble Data Assimilation System. *Mon. Weather. Rev.* **2013**, *141*, 754–772. [CrossRef]
20. Paul, S.; Ghosh, S.; Oglesby, R.; Pathak, A.; Chandrasekharan, A.; Ramsankaran, R. Weakening of Indian summer monsoon rainfall due to changes in land use land cover. *Sci. Rep.* **2016**, *6*, 32177. [CrossRef] [PubMed]
21. Meng, X.; Lyu, S.; Zhang, T.; Zhao, L.; Li, Z.; Han, B.; Li, S.; Ma, D.; Chen, H.; Ao, Y.; et al. Simulated cold bias being improved by using MODIS time-varying albedo in the Tibetan Plateau in WRF model. *Environ. Res. Lett.* **2018**, *13*, 044028. [CrossRef]
22. Kim, D.-H.; Kim, H.M. Effect of data assimilation in the Polar WRF with 3DVAR on the prediction of radiation, heat flux, cloud, and near surface atmospheric variables over Svalbard. *Atmos. Res.* **2022**, *272*, 106155. [CrossRef]
23. Ran, L.; Gilliam, R.; Binkowski, F.S.; Xiu, A.; Pleim, J.; Band, L. Sensitivity of the Weather Research and Forecast/Community Multiscale Air Quality modeling system to MODIS LAI, FPAR, and albedo. *J. Geophys. Res. Atmos.* **2015**, *120*, 8491–8511. [CrossRef]
24. Ran, L.; Pleim, J.; Gilliam, R.; Binkowski, F.S.; Hogrefe, C.; Band, L. Improved meteorology from an updated WRF/CMAQ modeling system with MODIS vegetation and albedo. *J. Geophys. Res. Atmos.* **2016**, *121*, 2393–2415. [CrossRef]
25. Ran, L.; Pleim, J.; Song, C.; Band, L.; Walker, J.T.; Binkowski, F.S. A photosynthesis-based two-leaf canopy stomatal conductance model for meteorology and air quality modeling with WRF/CMAQ PX LSM. *J. Geophys. Res. Atmos.* **2017**, *122*, 1930–1952. [CrossRef]
26. NASA. MODIS Design. Available online: https://modis.gsfc.nasa.gov/about/design.php (accessed on 1 November 2023).
27. Schaaf, C.W.Z. MCD43A1 MODIS/Terra+Aqua BRDF/Albedo Model Parameters Daily L3 Global–500 m V061. NASA EOSDIS Land Processes DAAC. Available online: https://ladsweb.modaps.eosdis.nasa.gov/missions-and-measurements/products/MCD43A1 (accessed on 1 November 2023).
28. Lyapustin, A.W.Y. MCD19A1 MODIS/Terra+Aqua Land Surface BRF Daily L2G Global 500 m, 1 km and 10 km SIN Grid. NASA LP DAAC. Available online: https://ladsweb.modaps.eosdis.nasa.gov/missions-and-measurements/products/MCD19A1 (accessed on 1 November 2023).
29. Lyapustin, A.W.Y. MCD19A2 MODIS/Terra+Aqua Aerosol Optical Thickness Daily L2G Global 1 km SIN Grid. NASA LP DAAC. Available online: https://ladsweb.modaps.eosdis.nasa.gov/missions-and-measurements/products/MCD19A2 (accessed on 1 November 2023).
30. Hall, D. MOD10A1/MYD10A1 Snow Products. Available online: https://modis-snow-ice.gsfc.nasa.gov/?c=MOD10A1 (accessed on 1 November 2023).
31. Myneni, R.K.; Taejin, P. MOD15A3H MODIS/Combined Terra+Aqua Leaf Area Index/FPAR Daily L4 Global 500 m SIN Grid. NASA LP DAAC. Available online: https://ladsweb.modaps.eosdis.nasa.gov/missions-and-measurements/products/MCD15A3H (accessed on 1 November 2023).
32. Vermote, E.; Tanré, D.; Deuzé, J.; Herman, M.; Morcrette, J.; Kotchenova, S. Second Simulation of a Satellite Signal in the Solar Spectrum–Vector. 6SV, 6S User Guide Version 3. 2006. Available online: https://ltdri.org/files/6S/6S_Manual_Part_1.pdf (accessed on 1 November 2023).
33. Mansfield, M.; Tran, H.; Tran, T. *2017 ARMS—Photochemical Grid Model Performance Evaluation for Base Year 2011*; Technical Report; Bureau of Land Management Utah Office, Utah State University—Bingham Research Center: Vernal, UT, USA, 2020; p. 66.
34. Helmig, D.; Ganzeveld, L.; Butler, T.; Oltmans, S.J. The role of ozone atmosphere-snow gas exchange on polar, boundary-layer tropospheric ozone—A review and sensitivity analysis. *Atmos. Chem. Phys.* **2007**, *7*, 15–30. [CrossRef]
35. National Operational Hydrologic Remote Sensing Center. *Snow Data Assimilation System (SNODAS) Data Products at NSIDC, Version 1*; National Snow and Ice Data Center: Boulder, CO, USA, 2004. [CrossRef]